



A Summary of the Microstructural Characterization Results for the A709 Commercial Heats

August 2023

Tate Patterson and Ting-Leung Sham
Idaho National Laboratory

Yanli Wang
Oak Ridge National Laboratory



*INL is a U.S. Department of Energy National Laboratory
operated by Battelle Energy Alliance, LLC*

DISCLAIMER

This information was prepared as an account of work sponsored by an agency of the U.S. Government. Neither the U.S. Government nor any agency thereof, nor any of their employees, makes any warranty, expressed or implied, or assumes any legal liability or responsibility for the accuracy, completeness, or usefulness, of any information, apparatus, product, or process disclosed, or represents that its use would not infringe privately owned rights. References herein to any specific commercial product, process, or service by trade name, trade mark, manufacturer, or otherwise, does not necessarily constitute or imply its endorsement, recommendation, or favoring by the U.S. Government or any agency thereof. The views and opinions of authors expressed herein do not necessarily state or reflect those of the U.S. Government or any agency thereof.

A Summary of the Microstructural Characterization Results for the A709 Commercial Heats

**Tate Patterson and Ting-Leung Sham
Idaho National Laboratory
Yanli Wang
Oak Ridge National Laboratory**

August 2023

**Idaho National Laboratory
Advanced Reactor Technologies
Idaho Falls, Idaho 83415**

<http://www.art.inl.gov>

**Prepared for the
U.S. Department of Energy
Office of Nuclear Energy
Under DOE Idaho Operations Office
Contract DE-AC07-05ID14517**

Page intentionally left blank

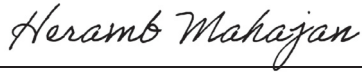
INL ART Program

A Summary of the Microstructural Characterization Results for the A709 Commercial Heats

INL/RPT-23-74406
Revision 0

August 2023

Technical Reviewer: (Confirmation of mathematical accuracy, and correctness of data and appropriateness of assumptions.)



Heramb P. Mahajan
Materials Engineer

8/29/2023

Date

Approved by:



Michael E. Davenport
ART Project Manager

8/29/2023

Date



Travis R. Mitchell
ART Program Manager

8/30/2023

Date



Michelle T. Sharp
INL Quality Assurance

8/29/2023

Date

Page intentionally left blank

ABSTRACT

To improve high temperature strength for advanced nuclear reactors, it is necessary to qualify additional structural materials for introduction into the American Society of Mechanical Engineers Boiler and Pressure Vessel Code. Specifically, Alloy 709 was identified as a material for Sodium-cooled Fast Reactors to enhance time-dependent mechanical properties compared to 316H stainless steel, a code qualified high temperature alloy. Idaho National Laboratory and Oak Ridge National Laboratory performed initial microstructure characterization and mechanical-property testing on a third commercial heat of Alloy 709 stainless steel. The solution-annealed Alloy 709 plate was produced by ATI Specialty Rolled Products. The chemical composition was within the limits for an American Society of Testing and Materials (ASTM) A213/A213M-23 specification for seamless tube for material UNS S31025. The grain size distribution of this heat was measured and an average grain size corresponding to ASTM Grain Size No. 6.5 was found. This met the minimum grain size limit corresponding to ASTM Grain Size No. 7 per ASTM A213 for seamless tube. The room-temperature tensile tests and hardness data also met the ASTM A213 specification. Creep-fatigue results on solution annealed plate material from the third commercial heat showed similar behavior to previous heats of Alloy 709. The characterization results and baseline mechanical properties of all three Alloy 709 commercial heats are summarized. It was recommended that all three commercial heats, after the application of a precipitation treatment of 1427°F (775°C) for 10 hours, can be used to generate data for the code qualification of Alloy 709.

Page intentionally left blank

ACKNOWLEDGEMENTS

This work was sponsored by the United States (US) Department of Energy (DOE) under Contract No. DE-AC07-05ID14517 with Idaho National Laboratory (INL), which is managed by Battelle Energy Alliance, and under Contract No. DE-AC05-00OR22725 with Oak Ridge National Laboratory, which is managed and operated by UT-Battelle LLC. Programmatic direction was provided by the Office of Nuclear Reactor Deployment of the DOE Office of Nuclear Energy (NE). The authors gratefully acknowledge the support provided by Sue Lesica of DOE-NE, Federal Materials Lead for the Advanced Reactor Technologies (ART) Program; Kaatrin Abbott of DOE-NE, Federal Manager, ART Fast Reactor Program (FRP); Bo Feng of Argonne National Laboratory, National Technical Director, ART FRP. The authors also acknowledge support from Richard Wright of Structural Alloys, LLC. The authors also thank Wesley Jones of INL for his support.

Page intentionally left blank

CONTENTS

ABSTRACT.....	vii
ACKNOWLEDGEMENTS.....	ix
ACRONYMS/ABBREVIATIONS.....	xv
1. MOTIVATION	1
2. EXPERIMENTAL METHODS.....	2
2.1. Chemical Analysis	2
2.2. Microstructure Characterization.....	3
2.3. Mechanical Testing.....	3
2.3.1. Tensile Testing.....	3
2.3.2. Hardness Testing.....	4
2.3.3. Fatigue and Creep-Fatigue Testing	4
3. RESULTS AND DISCUSSION	4
3.1. Chemical Composition.....	4
3.2. Microstructure Analysis.....	5
3.3. Mechanical Testing	8
3.3.1. Hardness.....	8
3.3.2. Tensile Testing.....	9
3.3.3. Fatigue Testing.....	10
3.3.4. Creep-Fatigue Testing.....	11
4. ALL THREE COMMERCIAL HEATS	11
4.1. Cyclic Properties	13
5. SUMMARY	14
6. REFERENCES.....	15

FIGURES

Figure 1. Image of the ATI-2 plates for the third commercial heat [10] and schematic showing the approximate plate dimensions for Heat 530843-02, Plate CG45192, and the extraction location for microstructure analysis (CG45192A8).....	2
Figure 2. Schematic with the approximate extraction and analysis locations and orientations in reference to the plate rolling direction and thickness.	2
Figure 3. Light optical micrographs of the transverse view (left) and longitudinal view (right) captured near the center of the plate thickness (middle half of the plate) as shown in Figure 2.....	5
Figure 4. Light optical micrographs of plan-view orientations from opposing sides of the plate 5 mm from the plate surface.	5
Figure 5. Photomicrograph showing (left) large, intergranular Nb precipitates and fine, intragranular precipitates and (right) dark field imaging revealing the compositional banding and precipitates with the rolling direction, from left to right.....	6
Figure 6. EBSD inverse pole figure (IPF) maps showing the grains and grain orientations for (top left) the transverse-, (top right) longitudinal-, and (bottom) plan-view orientations (bottom).	6
Figure 7. Grain size distributions for the transverse and longitudinal views shown in Figure 6.....	7
Figure 8. Secondary electron image showing Alloy 709 precipitates.....	7
Figure 9. EDS element concentration maps showing depletion of iron, chromium, and nickel, and enrichment of niobium and molybdenum for the large precipitates.	8
Figure 10. Longitudinal orientation microstructure showing the variation in grain size from the plate edge (left) towards the plate center (right) for 7.5 mm from the plate surface.	9
Figure 11. Hardness map using micro-Vickers at a 300 g load through the plate thickness.	9
Figure 12. Room-temperature tensile test engineering stress versus strain for Alloy 709 in the SA condition.	10
Figure 13. Peak stresses versus cycles for the Alloy 709 plate's (CG45192) elevated-temperature fatigue tests.	10
Figure 14. Peak stresses versus cycles for the Alloy 709 Plate (CG45192) creep-fatigue tests.	11
Figure 15. Cyclic data for the Alloy 709-PT materials from the three commercial heats shown in the format of the Section III, Division 5 creep-fatigue interaction diagram.....	14

TABLES

Table 1. Plate CG45192 tensile test specimen dimensions prior to testing.	3
Table 2. Chemical composition of Alloy 709, Heat 530843-02, Plate CG45192, reported in weight percent with an iron balance.	4
Table 3. Alloy 709 Plate CG45192 room-temperature tensile testing data and comparison to ASTM S31025 requirements.	9
Table 4. Fatigue testing parameters and results for Alloy 709 Plate CG45192.	10
Table 5. Creep-fatigue testing parameters and results for Alloy 709 Plate CG45192.	11
Table 6. Information on the three Alloy 709 commercial heats.	11
Table 7. Nominal chemical compositions of the three commercial heats of Alloy 709 (in wt.%).	12
Table 8. Average Vickers hardness values from the three commercial heats.	12
Table 9. Grain size overcheck for the three commercial heats.	13
Table 10. Average room temperature tensile properties of Alloy 709 in the solution annealed condition.	13

Page intentionally left blank

ACRONYMS/ABBREVIATIONS

ANL	Argonne National Laboratory
ART	Advanced Reactor Technologies
AOD	argon-oxygen decarburization
ASME	American Society of Mechanical Engineers
ASTM	American Society for Testing and Materials
ATI	Allegheny Technologies Incorporated
BPVC	Boiler and Pressure Vessel Code
DOE	Department of Energy
EBS	electron backscattered diffraction
EDS	energy dispersive spectroscopy
FR	fast reactors
FY	fiscal year
ICP-OES	inductively coupled plasma optical emission spectroscopy
ID	identification
IGA	instrumental gas analysis
INL	Idaho National Laboratory
MTR	material test record
ORNL	Oak Ridge National Laboratory
SEM	scanning electron microscope
UNS	unified numbering system
US	United States
UTS	ultimate tensile strength
YS	yield strength

Page intentionally left blank

A Summary of the Microstructural Characterization Results for the A709 Commercial Heats

1. MOTIVATION

Additional materials capable of withstanding the environmental conditions imposed by high temperature reactors are crucial to further the efficiencies and improve the designs of nuclear reactors and secure the United States' (US's) energy future. One of the advanced nuclear reactor designs to help tackle energy production challenges is the sodium-cooled fast reactor (SFR), which is proposed to operate at temperatures around 550°C [1].

The objective of advanced-materials development within the Fast Reactors Campaign of the Advanced Reactor Technologies (ART) Program, Department of Energy (DOE), Office of Nuclear Energy (NE), is to develop and qualify advanced structural materials that enable improved reactor performance. Improved structural-material performance can reduce costs of fast reactors by potentially allowing both higher operating temperatures (and thus, higher thermal efficiency and power output) and longer lifetimes for components. Improved materials reliability could also result in reduced downtime. Superior structural materials will also spur improvements in high-temperature design methodology, thereby allowing more flexibility in construction and operation. Advancements in material performance enable greater safety margins and more stable performance over a longer lifetime.

A multi-laboratory effort—involving the Argonne National Laboratory (ANL), the Idaho National Laboratory (INL), and Oak Ridge National Laboratory (ORNL)—was initiated to conduct alloy optimization and properties evaluation. Alloy 709 is an austenitic stainless steel (SS) containing nearly 20 wt% Cr and 25 wt% Ni, with intentional additions of Mo, Nb, Ti, and N. Based on Alloy 709's mechanical property performance compared to 316H SS, Alloy 709 was recommended by the three-lab team for qualification in the American Society of Mechanical Engineers (ASME) Boiler and Pressure Vessel Code (BPVC) Section III, Division 5 [2], which provides the construction rules for advanced-reactor components operating in the creep regime under cyclic service. A staged code-qualified construction material for advanced-reactor systems was developed, and a description of the test plan can be found in Reference [3].

Currently, the ART Program is generating Alloy 709 data to support the development of Section III, Division 5, code cases per the staged code qualification plan. Section III, Division 5, requires design data from a minimum of three commercial heats. Previous efforts have characterized two of the three commercial heats, and prior data can be found in references [4–9].

The objective of this work is to perform an initial characterization of the microstructure and mechanical properties of the third commercial heat of Alloy 709 in the solution-annealed condition, and to summarize the characterization results and baseline mechanical properties of all three Alloy 709 commercial heats.

A photograph of the third heat of Alloy 709 plates is shown on the left in Figure 1. The nominal plate thickness analyzed in this investigation was 1.75 in. and the approximate dimensions and metallographic section location is shown on the right in Figure 1.

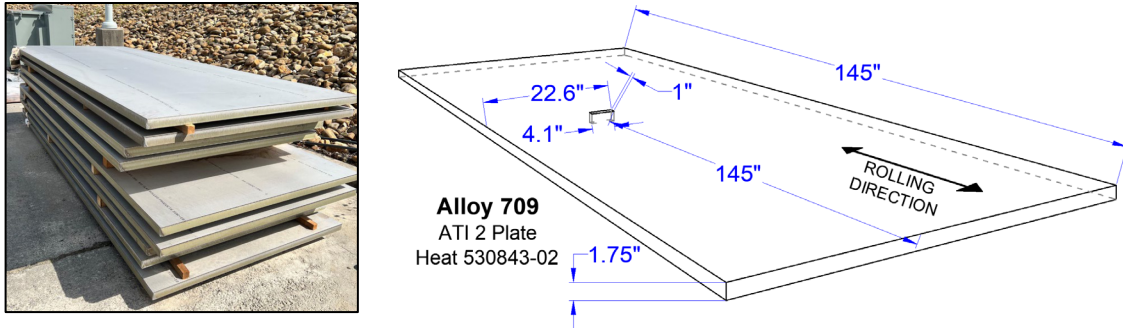


Figure 1. Image of the ATI-2 plates for the third commercial heat [10] and schematic showing the approximate plate dimensions for Heat 530843-02, Plate CG45192, and the extraction location for microstructure analysis (CG45192A8).

2. EXPERIMENTAL METHODS

The third commercial heat of Alloy 709 SS (UNS S31025) plate was procured from Allegheny Technologies, Incorporated (ATI). The plate was fabricated through the argon-oxygen decarburization (AOD) process, with electroslog remelting of 38,000 lb of material [10]. The vendor's heat of material identification was 530843-02. The plate was hot-rolled to a nominal thickness of 1.75 in, width of 56 in., and length of 145 in. The plate was solution-annealed (SA) at or above 1150°C, as defined in the American Society for Testing of Materials (ASTM) A213/A213M-23, "Standard Specification for Seamless Ferritic and Austenitic Alloy-Steel Boiler, Superheater, and Heat-Exchanger Tubes" [11]. An ASTM material specification does not exist for the plate form of Alloy 709. The vendor identification was CG45192 for this plate, and the SA condition was the only material condition analyzed in this report. Microstructural analysis was performed transverse to the rolling direction, longitudinal to the rolling direction, and via a plan view near the plate surfaces. A schematic with arrows indicating the view orientation is shown in Figure 2.

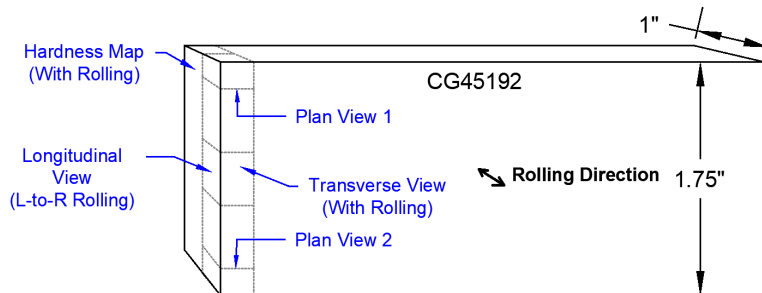


Figure 2. Schematic with the approximate extraction and analysis locations and orientations in reference to the plate rolling direction and thickness.

2.1. Chemical Analysis

Chemical analysis was performed using inductively coupled plasma optical emission spectroscopy (ICP-OES) for chromium, nickel, molybdenum, and manganese. Instrumental gas analysis (IGA) was used to measure carbon, nitrogen, and sulfur. Glow discharge mass spectroscopy (GDMS) was used for measuring all other reported element compositions. These measurements were performed based on ASTM A751-21 Standard Test Methods, Practices, and Terminology for Chemical Analysis of Steel Products [12] and ASTM E353-19 Standard Test Methods for Chemical Analysis of Stainless, Heat-Resisting, Maraging, and Other Similar Chromium-Nickel-Iron Alloys [13].

2.2. Microstructure Characterization

Microstructure characterization was performed using light optical microscopy and scanning electron microscopy (SEM). Specimen preparation was performed by hot mounting the sections in phenolic resin and grinding through successive reductions in SiC abrasive paper, followed by polishing using diamond suspensions down to 1 μm . Electrochemical etching with 10% oxalic acid and 6 V for approximately 30–90 sec was used to delineate the grain structure. Time varied based on the size of the specimen surface area (current density) and was lengthened as necessary to attain similar visual results for each cross-section. Photomicrographs were captured using a Keyence VHX-6000 confocal microscope using direct lighting. SEM was performed with a FEI Quanta 650 FEG scanning electron microscope (SEM). Backscattered electron (BSE) and electron backscattered diffraction (EBSD) images were captured with a FEI 6-channel BSD and MK2 amplifier and an EDAX Elect Plus (C5) camera. EBSD grain size analysis was performed using EDAX OIM Analysis software, where OIM stands for orientation imaging microscopy.

Due to the duplex grain size distribution and insufficient grain boundary delineation from chemical etching, the grain size measurement methods described in ASTM E112-13, “Standard Test Methods for Determining Average Grain Size,” [14] were not appropriate. Thus, the grain size analysis procedures were based on ASTM E2627-13, “Standard Practice for Determining Average Grain Size using Electron Backscattered Diffraction (EBSD) in Fully Recrystallized Polycrystalline Materials,” [15]. Techniques were also adapted from the procedures in following standards: ASTM E930-18, “Standard Test Methods for Estimating the Largest Grain Observed in a Metallographic Section (ALA Grain Size)” [16], E1181-02, “Standard Test Methods for Characterizing Duplex Grain Sizes” [17], and E1382-97, “Standard Test Methods for Determining Average Grain Size using Semiautomatic and Automatic Image Analysis” [18]. For comparison to historical grain size measurements and data, the grain size (diameter) measurements in microns were converted to an ASTM grain size number and rounded to the nearest half grain size.

2.3. Mechanical Testing

2.3.1. Tensile Testing

Tensile tests were performed in accordance with ASTM E8-21, “Standard Test Methods for Tension Testing of Metallic Materials” [19], using a cylindrical test specimen with a nominal 0.25 in. diameter and 1.250 in. length gage section. The yield strength was determined using 0.2% offset. The long axis of the tensile samples was parallel to and in the longitudinal direction of the plate. These tensile specimens were also centered relative to the plate thickness. The tensile tests were conducted at room temperature, and the testing parameters and measured dimensions for the two samples are shown in Table 1.

Table 1. Plate CG45192 tensile test specimen dimensions prior to testing.

Specimen ID	Temperature	Diameter (in.)	Gage Length (in.)
SAT-66	Ambient	0.249	1.2670
SAT-80	Ambient	0.250	1.2633

2.3.2. Hardness Testing

Hardness testing was performed according to ASTM E384-17, “Standard Test Method for Microindentation Hardness of Materials” [20]. Data was collected using a LECO LM247-AT automated hardness indenter at a 300-g load with a 13 sec dwell time. A matrix of hardness indentations was measured through most of the plate thickness, with the indentations oriented in the transverse view, as previously shown in Figure 2. A matrix consisting of 20 rows and 85 columns (1700 total indentations) was used, with 500 μm spacings between rows and columns. This produced a 10 mm \times 42.5 mm hardness test area or “map.” Sample preparation was performed by preparing the plate section in a 50 mm diameter mount using hot-pressed thermosetting phenolic resin. The sample was ground and polished to a 3 μm diamond suspension prior to indenting. Indents were performed in the as-polished (i.e., unetched condition). Following indenting, electrochemical etching was performed to capture micrographs.

2.3.3. Fatigue and Creep-Fatigue Testing

Fatigue and creep-fatigue specimens were extracted from the middle of the plate relative to thickness and oriented with the long axis parallel to the rolling direction. Fatigue testing was performed according to ASTM E606/E606M-21, “Standard Test Method for Strain-Controlled Fatigue Testing” [21], and creep-fatigue testing was performed according to ASTM E2714-13, “Standard Test Method for Creep-Fatigue Testing” [22]. Strain control for both tests was maintained with a fully reversed strain and total strain range of 1%. Fatigue and creep-fatigue tests were performed at two different temperatures of 1200°F (649°C) and 1500°F (816°C). The creep-fatigue test was held at peak strain for 30 minutes.

3. RESULTS AND DISCUSSION

3.1. Chemical Composition

The material test record (MTR) and measured chemical compositions are shown in Table 2. Table 2 also contains the allowable composition ranges for an UNS S31025 (Alloy 709) chemical composition according to ASTM A213/A213M-23, “Standard Specification for Seamless Ferritic and Austenitic Alloy-Steel Boiler, Superheater, and Heat-Exchanger Tubes” [11]. ASTM A213 is only for seamless tubes, but Alloy 709 in plate or sheet has not been introduced into ASTM A240/A240M-22a, “Standard Specification for Chromium and Chromium-Nickel Stainless Steel Plate, Sheet, and Strip for Pressure Vessels and for General Applications” [23]. The MTR and secondary chemical analyses showed agreement, and the measured composition is within the ASTM A213 composition ranges for each element analyzed.

Table 2. Chemical composition of Alloy 709, Heat 530843-02, Plate CG45192, reported in weight percent with an iron balance.

	Cr	Ni	Mo	Nb	Ti	Al	Cu
MTR	19.8	25.0	1.5	0.18	<0.01	0.02	0.05
Measurement	19.8	25.2	1.49	0.17	0.0008	0.016	0.030
ASTM A213 UNS S31025	19.5–23.0	23.0–26.0	1.0–2.0	0.10–0.40	0.20a	—	—
	C	N	Si	Mn	S	P	B
MTR	0.07	0.15	0.44	0.9	0.001	0.008	0.004
Measurement	0.073	0.15	0.29	0.94	<0.0005	0.0047	0.0026
ASTM A213 UNS S31025	0.10a	0.10–0.25	1.00a	1.50a	0.030a	0.030a	0.002– 0.010

^a Denotes maximum concentration.

3.2. Microstructure Analysis

Optical micrographs showing transverse and longitudinal views are shown as Figure 3. Microstructure banding was apparent when viewed in line with the rolling direction (transverse orientation) or from left to right (longitudinal orientation). The optical micrographs viewed into the thickness of the plate (plan-view orientation) are shown in Figure 4. Neither plan view orientations showed banding but both indicated large variations in grain size, as previously reported by McMurtrey et al. [9] and Bass and Sham [24]. Figure 5 shows a higher magnification of the microstructure and a dark-field micrograph. The left photomicrograph in Figure 5 shows the presence of large precipitates, typically concentrated along grain boundaries. Finer precipitates are apparent in the grain interiors with a relatively uniform distribution. The right micrograph delineates compositional/precipitate banding oriented with the rolling direction (left to right). For grain size analysis, EBSD was used for delineation of grain boundaries [15]. The EBSD inverse pole figure maps are shown in Figure 6.

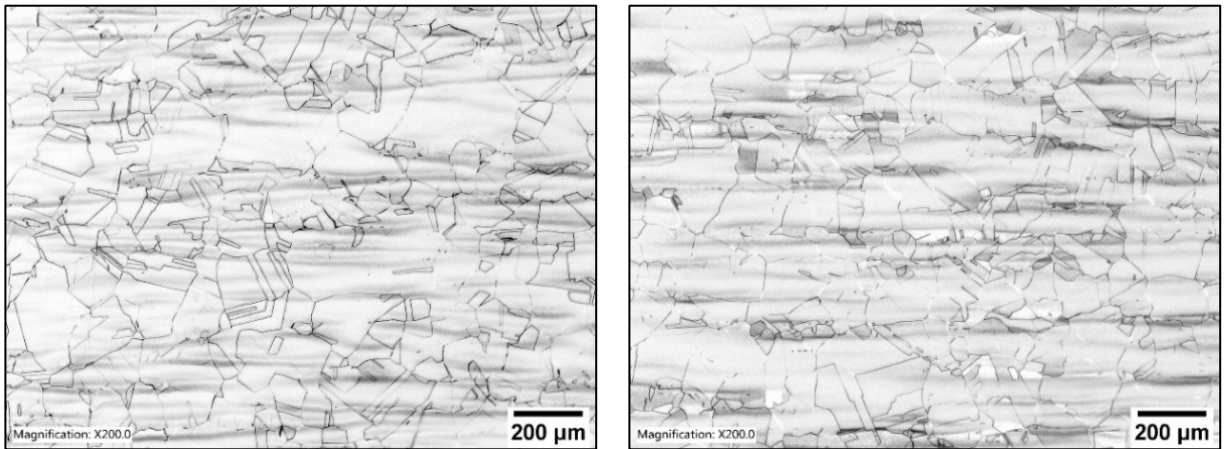


Figure 3. Light optical micrographs of the transverse view (left) and longitudinal view (right) captured near the center of the plate thickness (middle half of the plate) as shown in Figure 2.

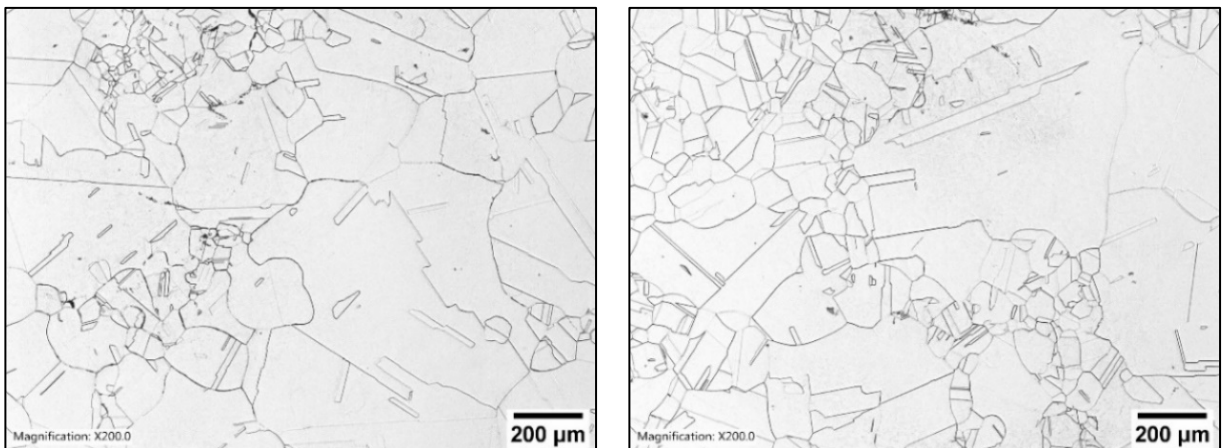


Figure 4. Light optical micrographs of plan-view orientations from opposing sides of the plate 5 mm from the plate surface.

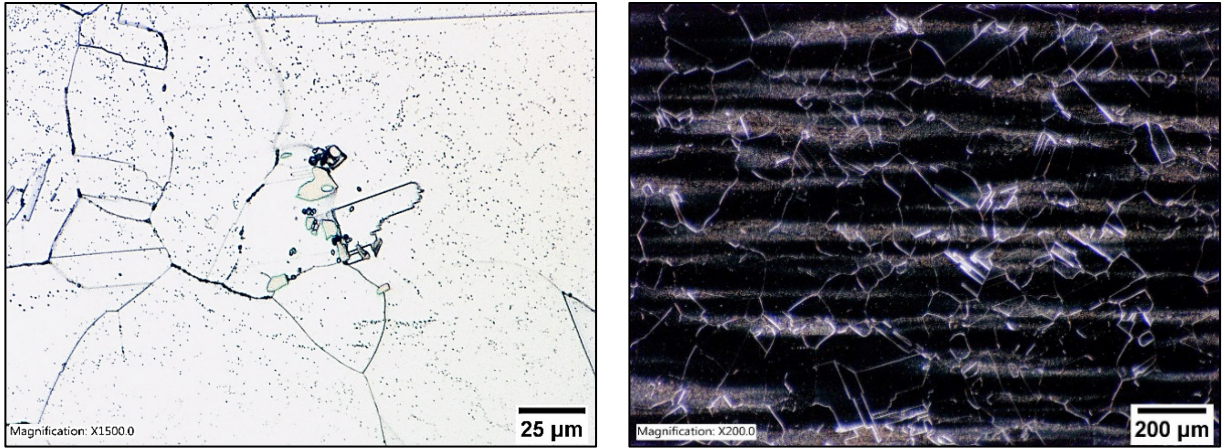


Figure 5. Photomicrograph showing (left) large, intergranular Nb precipitates and fine, intragranular precipitates and (right) dark field imaging revealing the compositional banding and precipitates with the rolling direction, from left to right. The micrographs were captured near the center of the plate.

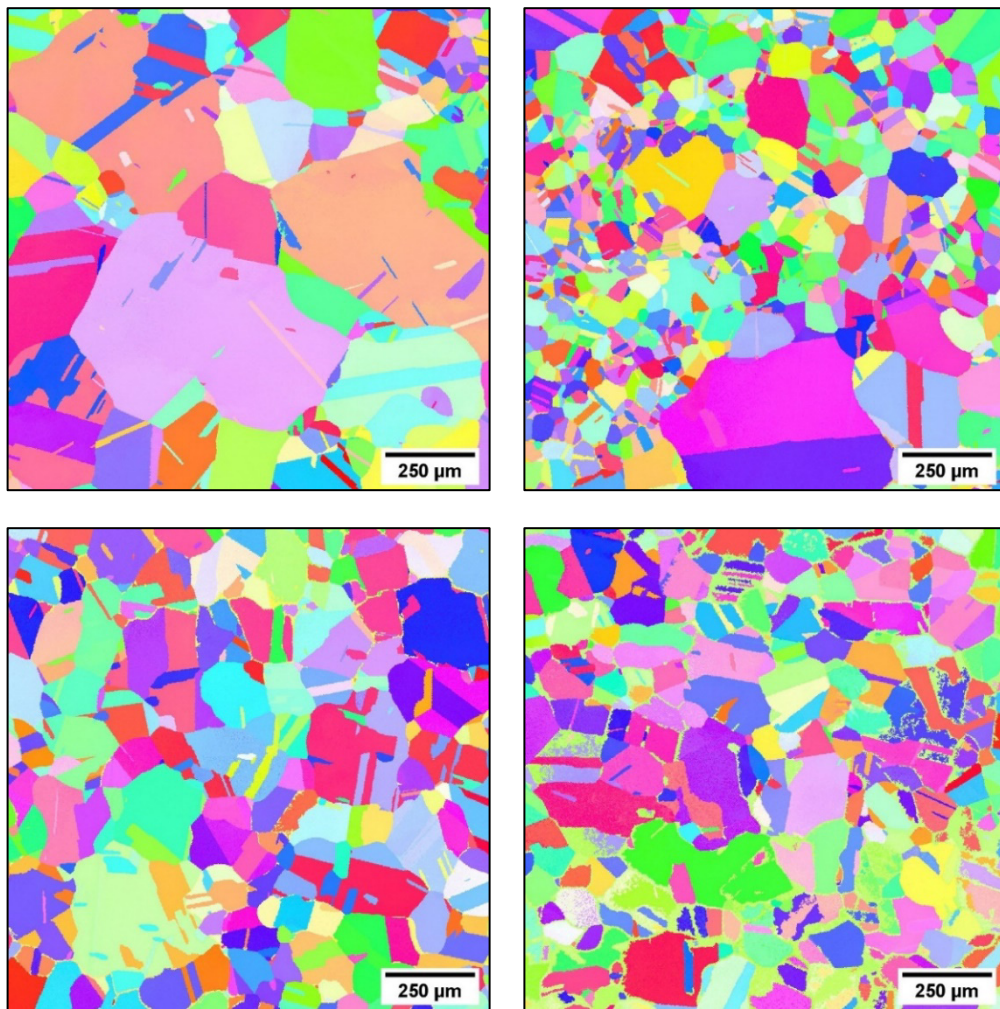


Figure 6. EBSD inverse pole figure (IPF) maps showing the grains and grain orientations for (top left) the transverse-, (top right) longitudinal-, and (bottom) plan-view orientations (bottom). Transverse and longitudinal views were captured near the plate center, more than 0.25 in. from the plate surface.

The views normal to the plate surface (transverse and longitudinal) appeared to have a more consistent grain size than views looking into the plate relative to the surface (plan view). The minimum grain size detected was 7 μm , but small grain diameters and twinning artifacts were not excluded from the EBSD IPF scans. The maximum grain size diameter was 536 μm (ASTM 00). The average grain size was computed to be approximately 38.6 μm (ASTM 6.5). This met the minimum grain size limit of 31.8 μm which corresponds to ASTM Grain Size No. 7 according to ASTM A213 [11] for UNS S31025. However, an average measurement is not representative of the material grain size due to the large variation in the microstructure, but an average allowed for comparing to ASTM 213 and previous work. The second commercial heat of Alloy 709 produced by ATI Specialty Rolled Products was reported to have an equiaxed grain size ranging from ASTM Grain Size No. 4 to 6 [24]. When evaluating only those micrographs from the middle half of the plate, the grain size distributions showed the largest area fraction of grains at a 110 μm diameter (ASTM Grain Size No. 3.5). The grain size distribution results are shown in Figure 7. These results are specific to the transverse and longitudinal views presented in Figure 6.

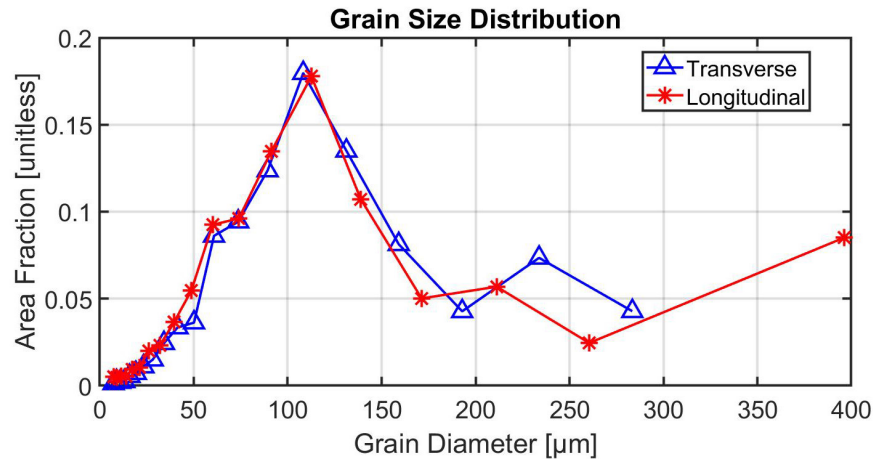


Figure 7. Grain size distributions for the transverse and longitudinal views shown in Figure 6.

For an approximation of precipitate size and chemical composition, a secondary electron image is shown in Figure 8. The energy dispersive spectroscopy (EDS) maps of qualitative element concentrations are shown in Figure 9. The precipitates were depleted of chromium, iron, and nickel, but enriched in niobium and molybdenum, and similar elemental enrichment was also shown for the fine precipitates, based on EDS point and line scans.

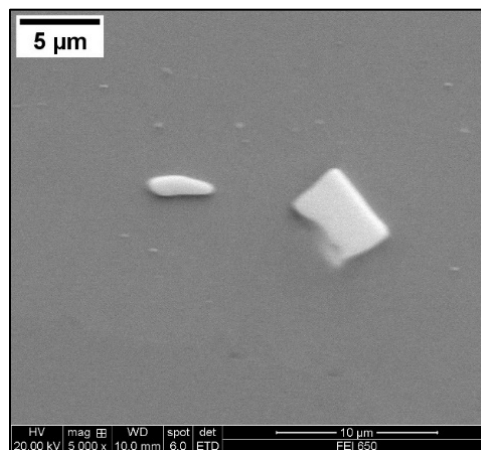


Figure 8. Secondary electron image showing Alloy 709 precipitates.

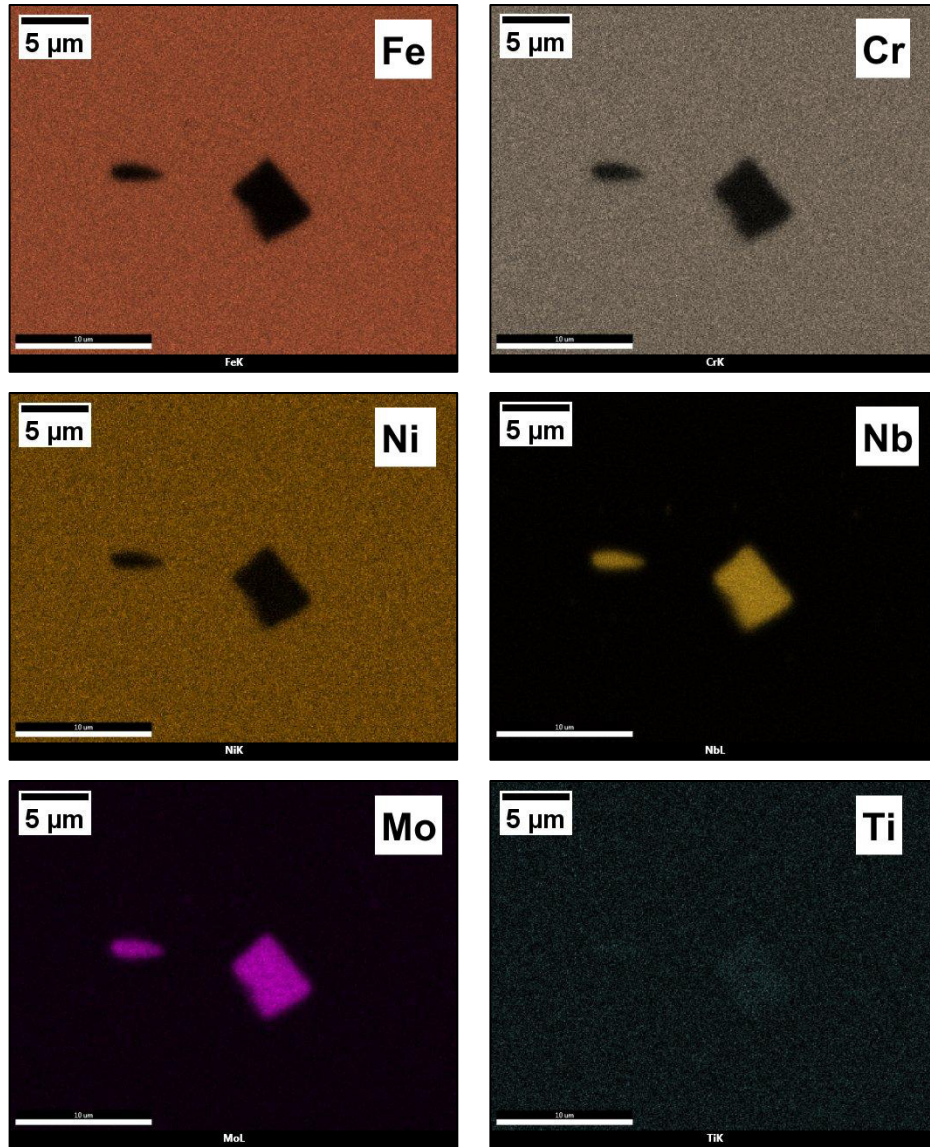


Figure 9. EDS element concentration maps showing depletion of iron, chromium, and nickel, and enrichment of niobium and molybdenum for the large precipitates.

3.3. Mechanical Testing

3.3.1. Hardness

Figure 10 shows a macrograph of the hardness indented specimen after indenting and etching in oxalic acid. From the surface of the plate (left side of photomicrograph) towards the plate interior (right side), an apparent grain size transition occurred nearly 5 mm below the plate surface. The maximum and minimum micro-Vickers hardness measurements using a 300-g load were 165 and 257 HV_{0.3}, respectively. This map is shown with a color/gray scale in Figure 11. The average hardness for the 1700 indents was 193 HV_{0.3}. ASTM A213 [11] mandates a maximum hardness of 270 HV for S31025, which is above the maximum hardness measured for any of the indents.

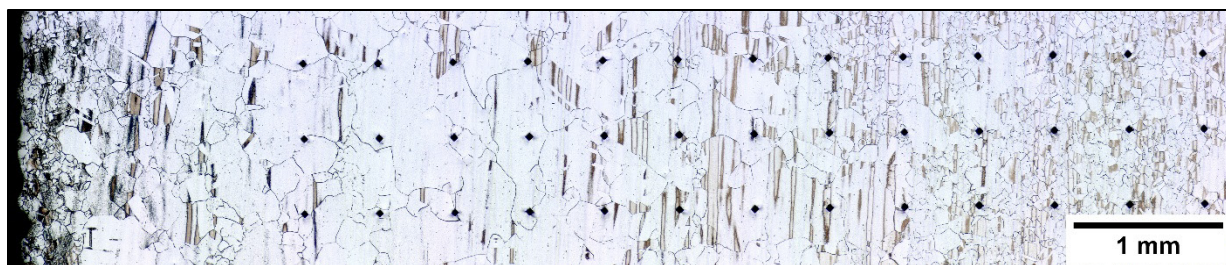


Figure 10. Longitudinal orientation microstructure showing the variation in grain size from the plate edge (left) towards the plate center (right) for 7.5 mm from the plate surface. The rolling direction is from top-to-bottom in the macrograph. Micro-Vickers hardness idents are present in this macrograph.

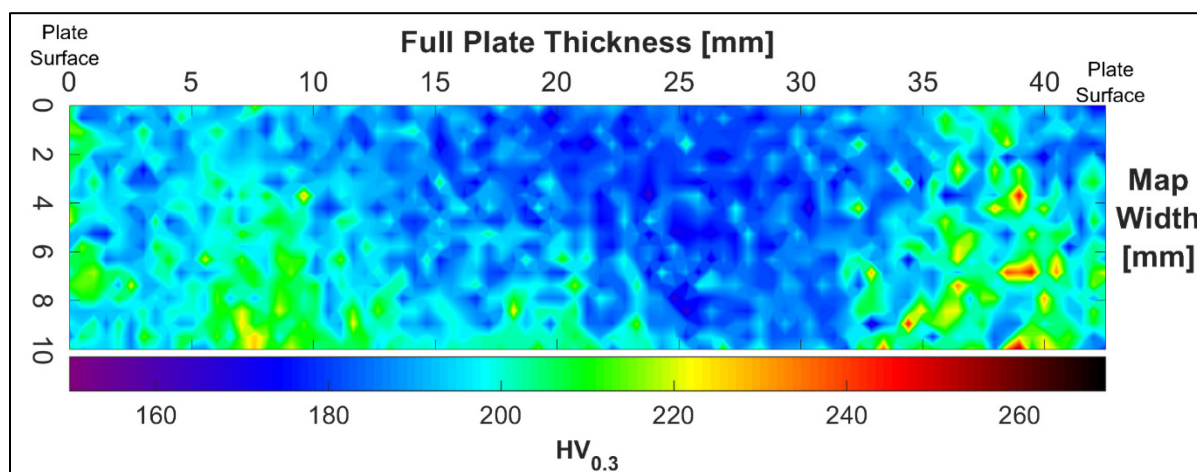


Figure 11. Hardness map using micro-Vickers at a 300 g load through the plate thickness. The rolling direction is in/out of page.

3.3.2. Tensile Testing

The measured room-temperature ($\approx 20^\circ\text{C}$) tensile testing data for the second heat of Alloy 709 (Plate CG45192) in the SA condition are shown in Table 3. The plotted engineering stress versus strain data are shown in Figure 12. The average yield strength (YS) and ultimate tensile strength (UTS) for both tests were 305 MPa (44.2 ksi) and 685 MPa (99.3 ksi), respectively.

Table 3. Alloy 709 Plate CG45192 room-temperature tensile testing data and comparison to ASTM S31025 requirements.

Specimen ID	Yield Strength 0.2% Offset (MPa)	Ultimate Tensile Strength (MPa)	Uniform Strain at UTS (%)	Total Strain at Break at Non-proportional Elongation (%)	Reduction of Cross-sectional Area (%)
SAT-66	313	688	35.8	46.1	72.5
SAT-80	296	681	39.1	49.0	73.0
ASTM UNS S31025	270 [min]	640 [min]	—	30 [min]	—

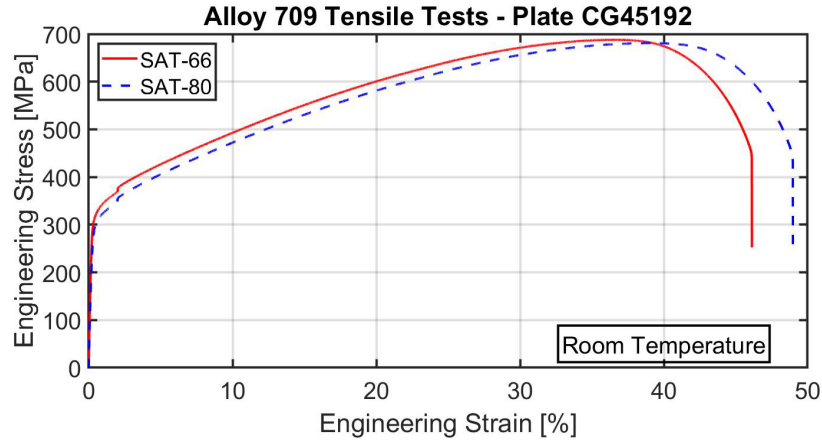


Figure 12. Room-temperature tensile test engineering stress versus strain for Alloy 709 in the SA condition.

3.3.3. Fatigue Testing

Elevated temperature fatigue testing results are shown in Table 4 at measured test temperatures of 649 and 816°C. The plot of peak stresses versus cycles for each test is shown in Figure 13. At a 649°C test temperature, the material withstood between 1334 and 1366 cycles before a 20% reduction in peak stress occurred. An increased test temperature to 816°C reduced the 20% stress reduction to nearly half: 595 cycles.

Table 4. Fatigue testing parameters and results for Alloy 709 Plate CG45192.

Test Temperature (°C)	Nominal Strain Range (%)	Strain Rate (s ⁻¹)	N ₀	N ₂₀ (max/min 20% drop)	Average Strain Range (%) *avg. until N ₀
649	1.00	1.0e-3	1002	1366	0.930
649	1.00	1.0e-3	936	1334	0.986
816	1.00	1.0e-3	411	595	0.990

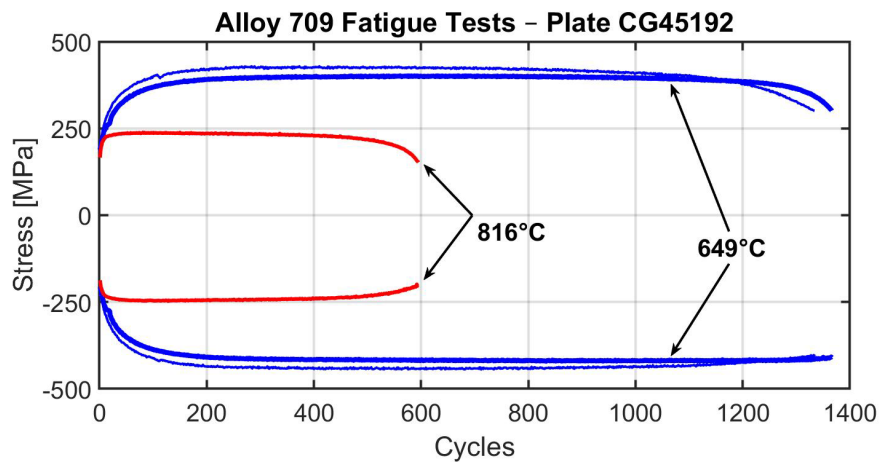


Figure 13. Peak stresses versus cycles for the Alloy 709 plate's (CG45192) elevated-temperature fatigue tests.

3.3.4. Creep-Fatigue Testing

Creep-fatigue tests were performed at 649 and 816°C, and the parameters are shown in Table 5. Figure 14 shows the plot of peak stresses versus cycles for both temperatures tested. The cycles to 20% drop in stress (N_{20}) at a 649°C test temperature was 260. This is lower than the nearly 375 cycles reported by Bass and Sham [24] for the second commercial heat of Alloy 709 from ATI. However, these results were similar to the results of the first commercial heat produced by G.O. Carlson, which showed cycles between approximately 200 and 275 at a 20% drop in stress.

Table 5. Creep-fatigue testing parameters and results for Alloy 709 Plate CG45192.

Test Temperature (°C)	Nominal Strain Range (%)	Hold Time (s)	Hold Type	Strain Rate (s^{-1})	N_0	N_{20} (max/min 20% drop)	Average Strain Range (%) *avg. until N_0
649	1.00	1800	Tension	1.0e-3	260	275	0.993
816	1.00	1800	Tension	1.0e-3	484	542	1.005

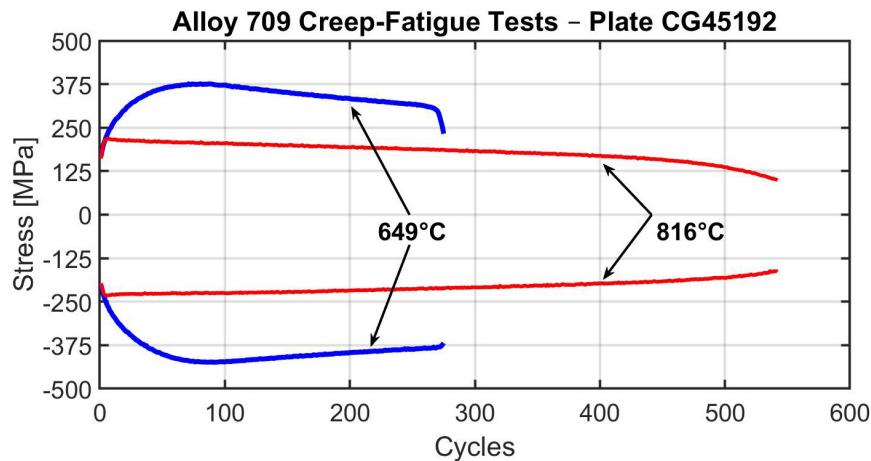


Figure 14. Peak stresses versus cycles for the Alloy 709 Plate (CG45192) creep-fatigue tests.

4. ALL THREE COMMERCIAL HEATS

The procurement of the three commercial heats for Alloy 709 satisfies the pre-requisite minimum number of commercial heats for generating design data to support the code qualification of Alloy 709 for ASME Section III, Division 5 Class A construction. This is a major accomplishment of the ART advanced materials program. Table 6 summarizes the specifics of these three commercial heats. The nominal ASTM Grain Size No. were provided by the fabricators.

Table 6. Information on the three Alloy 709 commercial heats.

Designation	Procurement Year	Fabricator	Master Heat #	Weight of Master Heat (lb)	Nominal ASTM Grain Size No.	Nominal Plate Thickness (in)
Carlson	FY 2017	G.O. Carlson Inc	58776	~ 45,000	7	1.1
ATI-1	FY 2021	ATI Specialty Rolled Products	529900	~ 40,000	7	1.75
					4	2.0
ATI-2	FY 2022		530843	~ 38,000	4	1.75

The processing parameters for the hot-rolled plates fabricated from these commercial heats are as follows. For the Carlson heat, there were nine combinations of melt practices and solution annealing temperatures. The three-lab team down-selected the electroslag remelting (ESR) melt practice and a solution annealing temperature of 1150°C (2102°F) from the Carlson heat to support the Alloy 709 code case testing. The hot-rolled plates fabricated from the ATI-1 and ATI-2 heats were based on ESR and a solution annealing temperature at or above 1150°C (2102°F).

The nominal chemical compositions of the three heats, as reported by the fabricators, are shown in Table 7. The laboratories conducted independent chemistry analysis and the results were consistent with the nominal chemical compositions provided by the fabricators.

Table 7. Nominal chemical compositions of the three commercial heats of Alloy 709 (in wt.%).

Element	Carlson	ATI-1	ATI-2	ASTM A213 UNS-S31025 Specification
C	0.066	0.08	0.07	0.10 max
Cr	20.05	19.9	19.8	19.5–23.0
Co	0.02	0.02	0.01	Not specified
Ni	25.14	24.6	25	23.0–26.0
Mn	0.9	0.9	0.9	1.50 max
Mo	1.51	1.5	1.5	1.0–2.0
N	0.152	0.15	0.15	0.10–0.25
Si	0.38	0.39	0.44	1.00 max
P	0.014	0.003	0.008	0.030 max
S	0.001	<0.001	0.001	0.030 max
Ti	0.01	<0.01	<0.01	0.20 max
Nb	0.26	0.17	0.18	0.10–0.40
Al	0.02	0.02	0.02	Not specified
B	0.003	0.004	0.005	0.002–0.010
Cu	0.06	0.06	0.04	Not specified

The average hardness values from the three commercial heats together with the maximum value from the specification are given in Table 8.

Table 8. Average Vickers hardness values from the three commercial heats.

	Carlson	ATI-1	ATI-2	ASTM A-213 UNS-S31025 Specification
Average Vickers Hardness (HV)	196	180	193	270 max

Grain size measurements were made by the three-laboratory team to verify the values provided by the fabricators. The average values of the ASTM Grain Size No. for the three commercial heats are tabulated in Table 9.

Table 9. Grain size overcheck for the three commercial heats.

	Carlson	ATI-1	ATI-2	Intended range of the ASTM Grain Size No. for the plate product form
Average ASTM Grain Size No.	7	5	6.5	4 to 7

The average room temperature tensile properties for the three heats in the solution annealed condition are shown in Table 10.

Table 10. Average room temperature tensile properties of Alloy 709 in the solution annealed condition.

Heat	Yield Stress (MPa)	Ultimate Tensile Stress (MPa)	Total elongation (%)
Carlson	287	664	49
ATI-1	312	685	49
ATI-2	305	685	48
ASTM A213 UNS-S31025 specification	270 min	640 min	30 min

The nominal chemical compositions, the average hardness values, and the average room temperature tensile properties for the three commercial heats all meet the ASTM A213 (UNS-S31025) specification requirements.

4.1. Cyclic Properties

Alloy 709 derives its enhanced creep strength from the precipitation of nano-sized carbonitride M(CN) particles on dislocations in a stable, fine dispersion as promoted by the time-at-temperature and the stress conditions during reactor plant operations. There is concern that formation of these precipitates will not happen for reactor operation temperatures that are at 975°F (525°C) or lower due to slow kinetics, and other detrimental phases may form instead. Based on computational materials simulations, two precipitation treatments were developed in [25]:

1. 1652°F (900°C) for 10 hours
2. 1472°F (775°C) for 10 hours

Microstructure analyses of precipitation treated samples showed that the 1472°F (775°C)/10 hours treatment gives the desirable microstructure, thus this precipitation treatment was selected [25].

Compared to solution annealing, aging reduces the amount of nitride or carbo-nitride forming elements in solution through precipitation of MX or Z phase prior to deformation. The precipitation treatment (PT) of 1472°F (775°C)/10 hours has resulted in reduced precipitation of MX or Z phases on dislocation substructures during subsequent cyclic deformation. The result is that there is less cyclic hardening compared to testing solution annealed material and the cycles to failure in creep-fatigue is significantly increased. The precipitation treatment does lead to a modest reduction in the creep rupture strength, but it gives a much more well-balanced set of design properties for advanced reactor structural applications.

The three-laboratory team has recommended to add this precipitation treatment for the Alloy 709 plates after a SA treatment at a temperature of 2102°F (1150°C) or higher as the baseline for developing

code qualification data for the Section III, Division 5 Alloy 709 Code Case. This material condition for code qualification will be referred to as Alloy 709-PT.

The cyclic data on fatigue and creep-fatigue generated to date for the Alloy 709-PT materials are shown in Figure 15 in the form of a Section III, Division 5 creep-fatigue interaction diagram, showing enhanced creep-fatigue properties for the Alloy 709-PT materials from the three commercial heats. The test temperatures of the cyclic data were from 1200°F (649°C) to 1742°F (950°C).

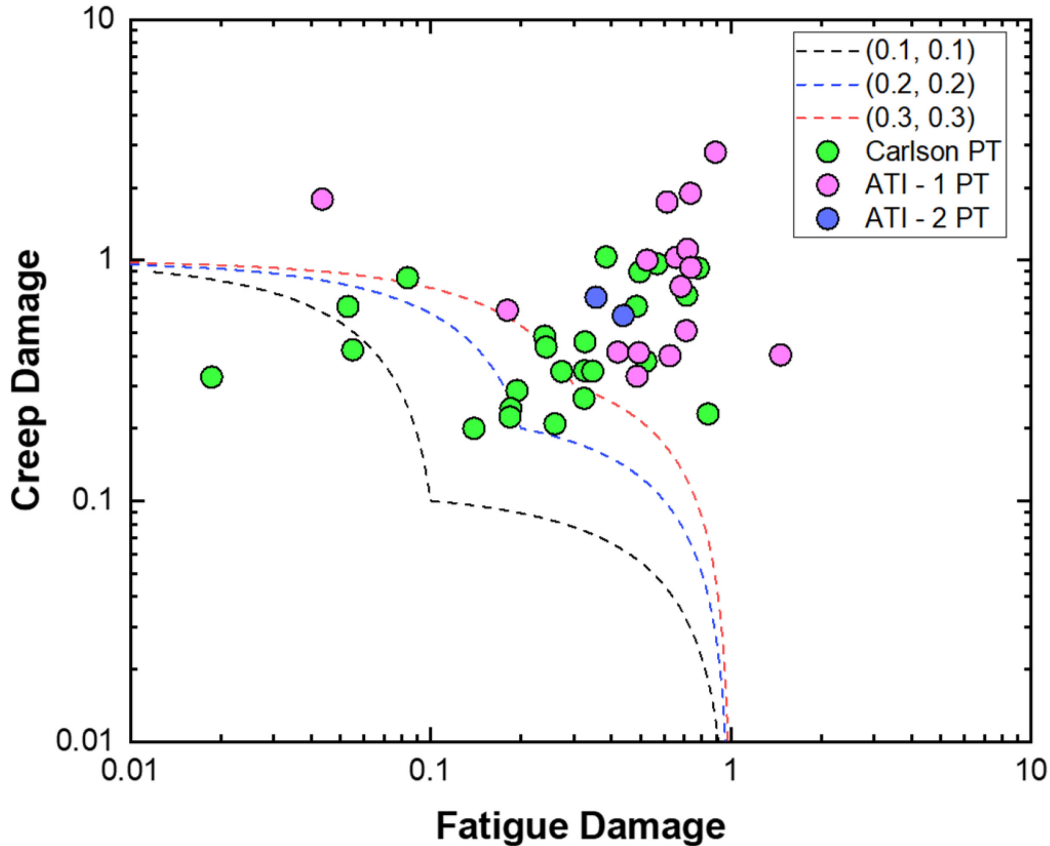


Figure 15. Cyclic data for the Alloy 709-PT materials from the three commercial heats shown in the format of the Section III, Division 5 creep-fatigue interaction diagram.

5. SUMMARY

This report contains the initial characterization of the third commercial heat of Alloy 709 in the SA condition. This work was performed to obtain baseline information, similar to the characterization of the second commercial heat in Reference [24], to support the Alloy 709 code qualification effort. The measured chemical composition was within the limits defined in ASTM A213 for seamless tube. The microstructural results revealed a large grain size distribution, similar to the other two commercial heats procured. The maximum grain size identified was approximately 536 μm in diameter (ASTM Grain Size No. 00), and the minimum grain size was approximately 7 μm (ASTM Grain Size No. 11). The full thickness hardness testing of the plate had an average hardness of 193 $\text{HV}_{0.3}$. The fatigue and creep-fatigue results showed performance similar to the previous Alloy 709 heats analyzed.

The characterization results and test data for the three Alloy 709 commercial heats are summarized. It is recommended that the Alloy 709-PT materials from the ATI-1 and ATI-2 heats, together with those

from the Carlson heat, can be used to generate the mechanical properties data for the code qualification of Alloy 709-PT.

6. REFERENCES

- [1] Ruggieri, J. M., *et al.* 2017. “Sodium-cooled Fast Reactor (SFR) System Safety Assessment.” GEN IV International Forum. https://www.gen-4.org/gif/upload/docs/application/pdf/2017-11/gif-sfr-safetyassessment-20170427_final.pdf. Ruggieri *et al* “Sodium-cooled Fast Reactor (SFR) System Safety Assessment” United States, 2021.
- [2] American Society of Mechanical Engineers. 2021. *ASME Section III Rules for Construction of Nuclear Facility Components, Division 5 High Temperature Reactors*. United States.
- [3] Sham, T.-L., and K. Natesan. 2017. “Code Qualification Plan for an Advanced Austenitic Stainless Steel , Alloy 709, for Sodium Fast Reactor Structural Applications.” In proceedings of International Conference on Fast Reactors and Related Fuel Cycles: Next Generation Nuclear for Sustainable Development (*FR17*), Yekaterinburg, Russian Federation, June 26 - 29, 2017. <https://www.iaea.org/publications/13414/fast-reactors-and-related-fuel-cycles-next-generation-nuclear-systems-for-sustainable-development-fr17>.
- [4] Wang, Y., P. Hou, and T.-L. Sham. 2021. “Report on FY 2021 Creep, Fatigue, and Creep-Fatigue Testing of Alloy 709 Base Metal at ORNL.” ORNL/TM- 2021/2120, Oak Ridge National Laboratory, Oak Ridge, Tennessee, USA. <https://doi.org/10.2172/1813151>.
- [5] Wang, Y., P. Hou, R. E. Bass, X. Zhang, and T.-L. Sham. 2022. “Interim Mechanical Properties Data from FY22 ORNL Testing of A709 with Precipitation Treatment for ASME Code Case Data Package.” ORNL/TM-2022/2593, Oak Ridge National Laboratory, Oak Ridge, Tennessee, USA. <https://doi.org/10.2172/1887676>.
- [6] Zhang, X., T.-L. Sham, and M. Li. 2021. “FY21 Status Report on Creep Rupture Testing at ANL to Support the Development of Alloy 709 Code Case.” ANL-ART-231, Argonne National Laboratory, Chicago, Illinois, USA. <https://doi.org/10.2172/1810715>.
- [7] Zhang, X., T. L. Sham, and G. A. Young. 2019. “Microstructural Characterization of Alloy 709 Plate Materials with Additional Heat Treatment Protocol.” ANL-ART-170. Argonne National Laboratory, Chicago, Illinois, USA. <https://doi.org/10.2172/1601459>.
- [8] Song, R., M. D. McMurtrey, and C. D. Clement. 2021. “Characterization of Alloy 709 Commercial Heats.” INL/EXT-21-64284, Idaho National Laboratory, Idaho Falls, Idaho, USA. <https://www.osti.gov/servlets/purl/1826588>.
- [9] McMurtrey, M., L. Carroll, and J. Wright. 2017. “Microstructural Effects on Creep-Fatigue Life of Alloy 709.” INL/EXT-17-41079, Idaho National Laboratory, Idaho Falls, Idaho, USA. <https://doi.org/10.2172/1404723>.
- [10] Wright, R. 2023. “A709 Procurement and ASTM Specification Status.” INL/MIS-23-72773, Idaho National Laboratory, Idaho Falls, Idaho, USA. <https://www.osti.gov/biblio/1984079>.
- [11] ASTM International. 2023. “*Standard Specification for Seamless Ferritic and Austenitic Alloy-Steel Boiler, Superheater, and Heat-Exchanger Tubes*.” ASTM A213/A213M-23.
- [12] ASTM International. 2021. “*Standard Test Methods, Practices, and Terminology for Chemical Analysis of Steel Products*.” ASTM A751-21.
- [13] ASTM International. 2019. “*Standard Test Methods for Chemical Analysis of Stainless, Heat-Resisting, Maraging, and Other Similar Chromium-Nickel-Iron Alloys*.” ASTM E353-19e1.
- [14] ASTM International. 2021. “*Standard Test Methods for Determining Average Grain Size*.” ASTM

- E112-13(2021).
- [15] ASTM International. 2019: “*Standard Practice for Determining Average Grain Size Using Electron Backscatter Diffraction (EBSD) in Fully Recrystallized Polycrystalline Materials.*” ASTM E2627-13(2019).
 - [16] ASTM International. 2018. “*Standard Test Methods for Estimating the Largest Grain Observed in a Metallographic Section (ALA Grain Size).*” ASTM E930-18.
 - [17] ASTM International. 2023. “*Standard Test Methods for Characterizing Duplex Grain Sizes.*” ASTM E1181-02(2015).
 - [18] ASTM International. 2023. “*Standard Test Methods for Determining Average Grain Size Using Semiautomatic and Automatic Image Analysis.*” ASTM E1382-97(2023).
 - [19] ASTM International. 2021. “*Standard Test Methods for Tension Testing of Metallic Materials.*” ASTM E8/E8M-21.
 - [20] ASTM International. 2017. “*Standard Test Method for Microindentation Hardness of Materials.*” ASTM E384-17.
 - [21] ASTM International. 2021. “*Standard Test Method for Strain-Controlled Fatigue Testing.*” ASTM E606/E606M-21.
 - [22] ASTM International. 2020. “*Standard Test Method for Creep-Fatigue Testing.*” ASTM E2714-13(2020).
 - [23] ASTM International. 2022. “*Standard Specification for Chromium and Chromium-Nickel Stainless Steel Plate, Sheet, and Strip for Pressure Vessels and for General Applications.*” ASTM A240/A240M-22a.
 - [24] Bass, R., and T.-L. Sham. 2022. “Initial Characterization of the Second A709 Commercial Heat.” INL/RPT-22-69073, Idaho National Laboratory, Idaho Falls, Idaho, USA. <https://www.osti.gov/biblio/1906451>.
 - [25] Zhang, X., T.-L. Sham, and G.A. Young. 2019. “Microstructural Characterization of Alloy 709 Plate Materials with Additional Heat Treatment Protocol.” ANL-ART-170, Argonne National Laboratory, Lemont, Illinois, USA. <https://www.osti.gov/biblio/1601459>.